New Limit for the Lepton-Family-Number Nonconserving Decay $\mu^+ \rightarrow e^+\gamma$

M. D. Cooper [Spokesman], M. L. Brooks, G. W. Hart, G. E. Hogan, M. A. Kroupa, L. J. Marek, and R. E. Mischke, (P-25); S. C. Wright (Chicago); P. S. Cooper (Fermilab); Y. K. Chen, M. Dzemidzic, A. Empl, E. V. Hungerford III, K. A. Lan, B. W. Mayes II, and W. H. von Witsch (Houston); J. E. Knott, K. M. Stantz, and J. J. Szymanski (Indiana); C. C. H. Jui and E. B. Hughes (Stanford); C. A. Gagliardi, R. E. Tribble, X. L. Tu, and L. A. Van Ausdeln (Texas A&M); D. D. Koetke, R. Manweiler, and T. D. S. Stanislaus (Valparaiso); K. O. H. Ziock (Virginia); and L. E. Piilonen (VPI)

Introduction

It is generally believed that the standard model that describes the electroweak force is a low-energy approximation to a more fundamental theory. Yet there is no clear experimental evidence either to guide its extension to additional physical processes or to predict the model parameters. One of these model assumptions is lepton family-number conservation, which has been empirically verified to high precision but is not a consequence of a known theory. Lepton family-number conservation is the idea, based on experimental observation, that the property of being an electron or a muon must be maintained even when particles transform through reactions; neutrino oscillations would be the first evidence that this principle is not absolute. Indeed many theoretical extensions to the standard model allow lepton-family-number violation within a range that can be tested by experiment.[1]

The predictions of the rate for a given family-number nonconserving process vary among these extensions, and the most sensitive process depends on the model. Many possibilities have been explored, and highly-precise experimental limits exist for a wide variety of processes. Of these, the rare muon decays have some of the lowest branching-ratio (BR) limits because muons can be copiously produced and have relatively long lifetimes. A BR is the fraction of a decay into a particular channel compared to all possible decays, and in the case of the muon, there is only one major mode, a muon decaying into an electron and two neutrinos [$\mu^+ \rightarrow e^+\nu_e\nu_\mu$]; this mode is referred to as normal muon decay. The rare process, $\mu^+ \rightarrow e^+\gamma$, is the classic example of a reaction that would be allowed except for muon and electron number conservation; there are no neutrinos to carry the family characteristic. The previous limit[2] is BR($\mu^+ \rightarrow e^+\gamma$) < 4.9×10^{-11}. This decay is particularly sensitive to the standard model extension that involves supersymmetric particles.[3]

We report here a new limit for the BR of the decay $\mu^+ \rightarrow e^+\gamma$ from the analysis of data taken by the MEGA experiment at the Los Alamos Meson Physics Facility, LAMPF (renamed LANSCE). The dominant source of background in high-rate $\mu^+ \rightarrow e^+\gamma$ experiments is random coincidences between high-energy positrons from the primary decay process, $\mu^+ \rightarrow e^+\nu_e\nu_\mu$, and high-energy photons from internal bremsstrahlung (IB), $\mu^+ \rightarrow e^+\gamma\nu_e\nu_\mu$. IB is normal muon decay modified by the emission of a photon by one of the charged particles. MEGA isolates the $\mu^+ \rightarrow e^+\gamma$ process from the background by identifying the signature of the process: a 52.8-MeV photon and a 52.8-MeV positron that are aligned back to back, in time coincidence, and arise from a common origin. These kinematic constraints arise from the conservation of momentum and energy for a particle at rest decaying into two others.

Experiment

Therefore, quality position, timing, and energy information are crucial. In comparison to the detector used to set the previous limit[2], the MEGA detector sacrifices larger acceptance and efficiency for better resolution, background rejection, and rate capability. It has been described in several papers[3,4] and will be discussed only briefly below.

Muons for the experiment are provided by a surface muon beam at the stopped-muon channel at LAMPF. Protons from the accelerator produce pions, and if these pions stop very close to the surface of the production target, they will decay to muons that can be transported and focused into a beam by a magnetic channel. The muons, which are nearly 100% polarized, are brought to rest in a 76 μm Mylar foil, centered in the 1.5-T magnetic field of a superconducting solenoid; see Figure 1. The angle between the muon beam and the normal to the target plane is 82.8° so that the stopping power in the beam direction is increased, while the thickness of material presented to the decay positrons is minimized. A sloped target plane also extends the stopping distribution along the beam, enhancing the sensitivity of the apparatus to the measurement of the decay position, which is the intersection of the outgoing photon and positron trajectories with the target foil.

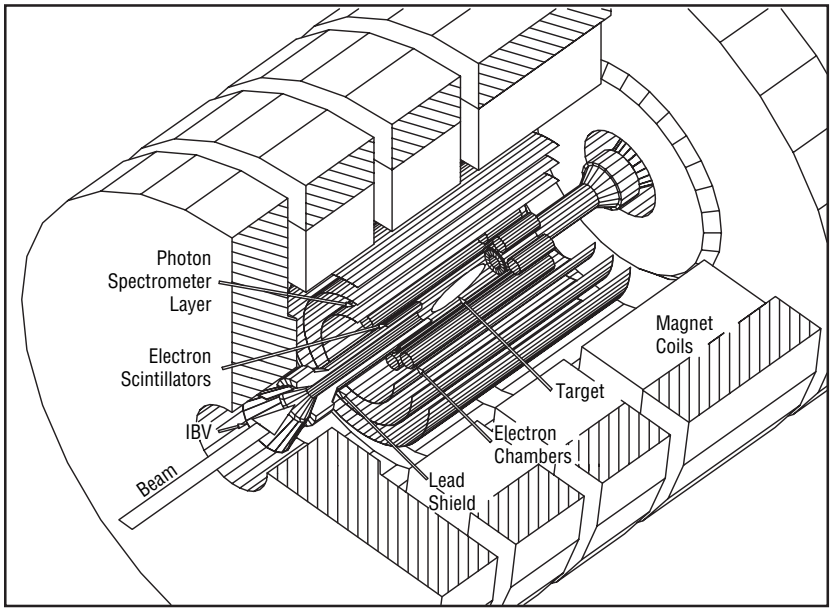

Figure 1. A simplified cutaway view of the MEGA apparatus. The detector is mounted inside a superconducting solenoid with a 1.5-T field. The muons enter along magnetic field and stop in the target. Positrons from muon decays are detected in the eight cylindrical wire chambers and the cylindrical arrays of scintillators surrounding the beam pipes. The three large cylinders are pair spectrometers for photon detection.

The positron and photon detectors are placed in the 1.8-m diameter and 2-m axial-length bore of the solenoid. Decay positrons from stopped muons are analyzed by a set of high-rate, cylindrical multiwire-proportional chambers (MWPC) that surround the target. A MWPC is a detector that measures the position of a particle that passes through it; ours have positively charged anode wires and grounded cathode foils. The set consists of seven MWPCs arranged symmetrically outside of a larger MWPC, coaxial with the central axis of the beam. These MWPCs have a thickness of 3×10^{-4} radiation lengths (an amount of matter that will induce with high probability the radiation of a photon by a charged particle), which minimize energy loss while maintaining high acceptance and efficiency under the stopping rates of the experiment.[3] The azimuthal location of a passing charged particle is determined by anode wire readout. The position of an event in the axial direction is obtained from the signal induced on stereo strips scribed on the inner and outer cathode foils of the MWPCs. The positrons come to rest at either end of the

spectrometer in thick, high-Z material after passing through a barrel of 87 scintillators used for measuring the time of passage of the positrons. Scintillators detect the passage of a charged particle by emitting visible light in proportion to the energy deposited in them. Outside these MWPCs, photons are detected in one of three coaxial, cylindrical pair spectrometers.[4] A pair spectrometer is a device that measures the kinematic properties of the electron and positron pair that may be produced when a photon interacts with matter. Each pair spectrometer consists of a scintillation barrel, two 250-μm Pb conversion foils that sandwich a MWPC, and three layers of drift chambers (similar to a MWPC), with the innermost having a delay-line readout to determine the axial position of a hit. The delay line determines the axial position by comparing the propagation time of the signal to each end. In this case, the line is highly folded to make the velocity of propagation slow, thus improving the precision of the position.

The hardware trigger indicates the occurrence of an interesting event; it consists of two stages of specially-constructed high-speed logic circuits, and is fed signals from each of the three photon spectrometers.[5] By using pattern recognition programmed on the basis of Monte Carlo (MC) simulations, the trigger requires an electron-positron pair that can be potentially reconstructed as arising from a photon of at least 37 MeV. Because the instantaneous muon stopping rate in this experiment is 250 MHz, with a macroscopic duty cycle of 6%–7%, the positron chambers and scintillators have too many hits at any given time to be part of the trigger. Signals are digitized in FASTBUS (an electronics module that meets proscribed circuit standards) with 6% dead time at the instantaneous trigger rate of 18 kHz. Between each macropulse (120 Hz) of the accelerator, the data are read into one of eight networked workstations, where an on-line algorithm reduces the data rate for storage on magnetic tape to roughly 60 Hz.

Each event is characterized by five kinematic parameters: photon energy (E_γ), positron energy (E_e), relative time between the positron and photon ($t_{e\gamma}$) at the muon decay point, opening angle ($\theta_{e\gamma}$), and photon traceback angle ($\Delta\theta_z$). These properties, in conjunction with the detector response, determine the likelihood that a signal is detected. The determination of the detector acceptance (the fraction of all decays observed by the detector) and response functions (the distribution of measured values for particle properties of a fixed value) relies on a MC simulation to extrapolate from experimental input to the kinematic region of the $\mu^+ \rightarrow e^+\gamma$ signal. To verify the MC calculation, a number of auxiliary measurements are performed. The two most important are the $\pi^-_{stopped} p \rightarrow \pi^0 n \rightarrow \gamma\gamma n$ process and the prompt e-γ coincidence signal from the IB decay.

Figure 2. The E_γ spectrum from photons converting in the outer layer of lead. The data points are produced by stopping pions in CH_2 via the reaction $\pi^-_{stopped} p \rightarrow \pi^0 n \rightarrow \gamma\gamma n$, scaled from 54.9 to 52.8 MeV. The curve is the response function generated from the MC and used in the analysis of the $\mu^+ \rightarrow e^+\gamma$ data.

Pion capture at rest on hydrogen produces photons with energies between 54.9 and 83.0 MeV, and such events have been collected using a loose-coincidence trigger. Under the condition that the two photons have a minimum opening angle of 173.5°, these photons are restricted to have energies close to 54.9 and 83.0 MeV respectively and a spread much smaller than the detector response. Figure 2 shows the experimental line shape for the 54.9 MeV photon for conversions in the outer Pb foils of the three pair spectrometers, scaled to 52.8 MeV. The curve is the response function generated from the MC that is used in the analysis of the $\mu^+ \rightarrow e^+\gamma$ data. The central energy and width of the distribution are well reproduced.

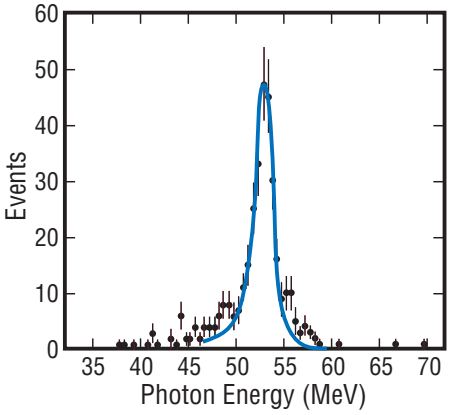

We attribute differences in the low-energy tail to charge exchange of in-flight pions from carbon in the CH_2 target and discrepancies in the high-energy tail to contributions from other opening angles due to special difficulties in conversion-point identification for the 83.0-MeV photon. The measured and simulated line shapes agree better for conversions in inner Pb foils, which have worse resolution. The energy resolutions are 3.3% and 5.7% full width at half maximum (FWHM) at 52.8 MeV for conversions in the outer and the inner Pb layers, respectively. The π^0 decays also provide the time response between the two photons, which is reasonably characterized by a Gaussian with a $\sigma = 0.57$ ns for each photon.

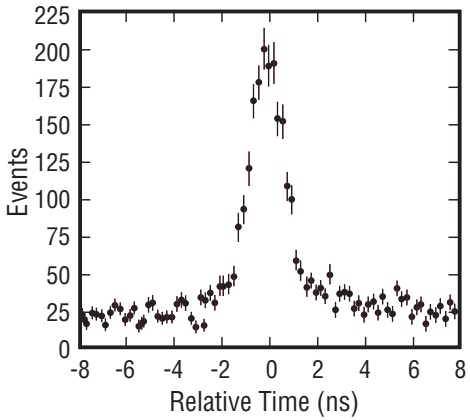

Figure 3. Values for $t_{e\gamma}$ from the process $\mu^+ \rightarrow e^+\nu_e\nu_\mu$ under the conditions of reduced rate and magnetic field.

Observation of the IB process demonstrates that the apparatus can detect coincident e-γ events. At nominal beam intensity, this process is completely engulfed by random coincidences. Figure 3 shows the spectrum for $t_{e\gamma}$, with the beam intensity reduced by a factor of 60, the magnetic field lowered by 25%, and the $\mu^+ \rightarrow e^+\gamma$ on-line filter suppressed. The peak shown is for all energies of the detected decay products. The area of the peak is very sensitive to the exact acceptances of the detector at its thresholds and can be calculated by MC simulation to better than a factor of two. If the data and the simulation are restricted to $E_\gamma > 46$ MeV, $E_e > 40$ MeV, and $\theta_{e\gamma} > 120°$, the BR is reproduced within 20%. The uncertainties of the IB normalization do not affect the precision of the $\mu^+ \rightarrow e^+\gamma$ acceptance because the IB prefers to occur near the energy-cut boundaries while the $\mu^+ \rightarrow e^+\gamma$ process occurs well above these cuts. The shape of the peak can be characterized by a Gaussian with a $\sigma = 0.77$ ns. The dominant contributor is the photon timing, as measured in the stopping-pion experiment, which must be scaled down from about 70 to 40 MeV for the comparison. At 52.8 MeV, the MC simulation indicates the photon-positron resolution is $\sigma = 0.68$ ns.

In the IB and $\mu^+ \rightarrow e^+\gamma$ processes, the origin of the photon is defined to be the intersection of the positron with the target. The photon traceback angle, $\Delta\theta_z$, specifies the difference between the polar angles of the photon as determined from the line connecting the decay point to the photon-conversion point and from the reconstructed e^+ - e^- pair. The resolution of $\Delta\theta_z$ is dominated by multiple scattering of the pair in the Pb converters. The observed response for inner and outer conversion layers for the IB process is in excellent agreement with the MC simulation. The traceback resolutions appropriate for the $\mu^+ \rightarrow e^+\gamma$ analysis are $\sigma = 0.067$ and 0.116 rad for conversions in the outer and the inner Pb layers, respectively.

The resolution of E_e is determined by the slope of the high-energy cut-off edge in the spectrum of the decay, $\mu^+ \rightarrow e^+\nu_e\nu_\mu$. It depends on the "topology" of the track, which is determined by the number of loops these particles make in the magnetic field between the target and scintillator and the number of chambers they traverse. The E_e spectrum is shown in Figure 4 for one of three topology groups. The

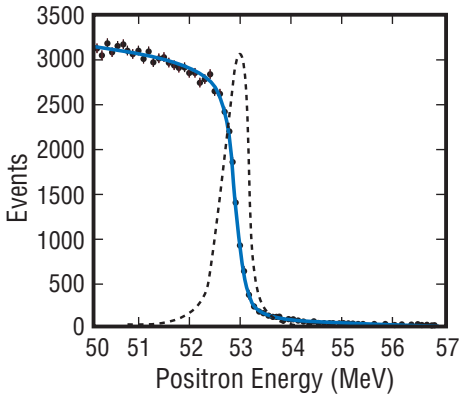

Figure 4. The E_e spectrum from $\mu^+ \rightarrow e^+\nu_e\nu_\mu$ extracted from full rate data for the middle topology group. The solid curve is the fit used to extract the line shape (dashed curve).

MC line shape is characterized near the centroid by a Gaussian and in the tails by different powers of the deviation from the central energy. To extract the response function from the data, this line shape is convoluted with the spectrum from normal muon decay, modified by detector acceptance and unphysical "ghost" tracks. Ghost tracks are a high-rate phenomenon and are reconstructions made from the fragments of several physical tracks. They are the source of events well above the kinematic limit for the positron energy. The solid curve in Figure 4 is the fit, and the dashed curve is the corresponding line shape. The central Gaussians of the three topology groups have σ = 0.21, 0.23, and 0.36 MeV.

There is no way to measure the response function for $\theta_{e\gamma}$. The MC simulation is relied upon to produce this distribution and gives the FWHM for $\cos(\theta_{e\gamma})$ as 1.21×10^{-4} at 180°. Given helical tracks, knowing the location of the target is critical to obtaining the correct absolute value of $\theta_{e\gamma}$, and the mechanical survey provides the most accurate measurement for the analysis.

Analysis

The data for this experiment have been taken in three calendar years, 1993–95. The full data set is based on 1.2×10^{14} muon stops collected over 8×10^6 s of live time and results in 4.5×10^8 events on magnetic tape. These events are passed through a set of computer programs that reconstruct as many as the pattern-recognition algorithms can interpret. The programs include physical effects such as mean energy loss in matter and nonuniformities in the magnetic field. The size of the data sample is reduced by cutting out events of poor quality or whose kinematic properties are far from those of a $\mu^+ \rightarrow e^+\gamma$ event. Events are required to satisfy separate χ_ν^2 (quality) cuts on the positron and photon fits and loose cuts on the signal kinematics ($E_e > 50$ MeV, $E_\gamma > 46$ MeV, $t_{e\gamma} < 4$ ns, $\cos(\theta_{e\gamma}) < -0.9962$, and $\Delta\theta_z < 0.5$ rad). Events in which the positron momentum vector at the decay point appears to lie within 5° of the plane of the target are discarded. After roughly one year of computing on a farm of UNIX workstations, the data set has been reduced to 3971 events that are fully reconstructed and of continuing interest. This sample is large enough to allow a study of the background. To remove incorrectly reconstructed events, the images of the photon showers in the pair spectrometers are manually scanned. The efficiency for keeping real photons is monitored by mixing about 500 52.8-MeV MC events into the sample in a nonidentifiable way and finding that 91% of the MC events pass, whereas only 73% of the data events are selected. Most of the excess data events that are rejected consist of two overlapping low-energy photon showers that have been reconstructed by the analysis program as a single high-energy shower.

The acceptance of the apparatus—which includes geometrical, trigger, and pattern-recognition constraints—is obtained by simulating 1.2×10^7 unpolarized $\mu^+ \rightarrow e^+\gamma$ decays and finding that 5.2×10^4 events survive processing by the same codes used for the data analysis. Thus the probability that a $\mu^+ \rightarrow e^+\gamma$ decay would be detected is 4.3×10^{-3}. This value is reduced by 9% for the inefficiency of manual scanning. The acceptance is further reduced by 20% to account for inadequacies in the MC simulation that overestimate the acceptance. The shortcomings primarily involve cross talk amongst channels of electronics and are estimated by comparing the images of many data and MC events to contribute only 4% to the overall uncertainty in the acceptance. The total number of muon stops is determined by calibrating the rates in the positron scintillators to a known muon flux. After correcting for dead time, the single event sensitivity for the experiment is $2.3 \pm 0.2 \times 10^{-12} = 1/N_\mu$, where N_μ is the number of useful stopped muons.

The determination of the number of $\mu^+ \rightarrow e^+\gamma$ events in the sample is evaluated using the likelihood method described in the analysis of previous experiments.[6] This likelihood analysis is analogous to a least-squares fit of data that contain two signals and a background but depends upon the properties of five independent variables. The analysis is carried out by evaluating the kinematic properties of each event and estimating the probability that that event is either $\mu^+ \rightarrow e^+\gamma$, IB, or background. The analysis uses the response function of the detector to each possibility. The total number of events is fixed at 3971. The number of $e^+\gamma$ events, $N_{e\gamma}$, and the number of IB events, N_{IB}, are treated as independent variables.

Results

The likelihood function evaluates the statistical separation between signal, IB, and background; it is maximal at the preferred values of the independent variables. To observe the impact of quality constraints in the pattern recognition, they have been relaxed to produce a sample three times larger. One event emerges with a large signal probability and is significantly separated from the distribution. However, this event has a large positron χ_{ν}^2, indicative of a ghost track. The adopted constraints produce a sample with considerably less background. The result presented below is stable against changes in the constraints; *e.g.*, the higher value of $N_{e\gamma}$ is compensated by a corresponding increase in acceptance. The contours of constant likelihood are shown in Figure 5. The peak of the likelihood function is at $N_{e\gamma} = 0$ and $N_{IB} = 30 \pm 8 \pm 15$. The systematic error assigned to N_{IB} is due to the uncertainty in the shape of the background time spectrum after the events are filtered by the on-line program. The expected number of IB events is $36 \pm 3 \pm 10$, where the systematic error is due to finite resolution effects across the cut boundaries.

The 90% confidence limit is the value for $N_{e\gamma}$ where 90% of the area of the likelihood curve lies below $N_{e\gamma}$ and N_{IB} is maximal. This value is $N_{e\gamma} < 5.1$. Therefore, the limit on the BR($\mu^+ \rightarrow e^+\gamma$) is $5.1/ N_{\mu} = 1.2 \times 10^{-11}$ with 90% confidence. In comparison to the previous experimental limit[2], this result represents a factor of 4.1 improvement. The previous experiment would have had 100 background events at the same BR instead of the 2 found here. The background level of 2 events is the mean value of a Poisson statistical distribution and may be made up of the probability tails of many events. This improvement further constrains attempts to build extensions to the standard model.[1] Grand-unified supersymmetric extensions to the standard model have many parameters, and this new limit on $\mu^+ \rightarrow e^+\gamma$ increases the appropriate masses by 40%.

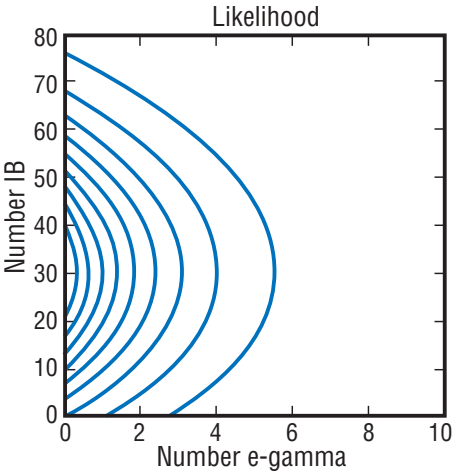

Figure 5. The contours of constant likelihood for the processes $\mu^+ \rightarrow e^+\gamma$ and $\mu^+ \rightarrow e^+\nu_e\nu_\mu$. The best estimate for the number of events in the final sample of each type is given by the coordinates where the likelihood function is a maximum.

References

[1] R. Barbieri, L. Hall, and A. Strumia, "Violations of Lepton Flavour and CP in Supersymmetric Unified Theories," *Nuclear Physics B*, 455, 219–251 (1995);

N. Arkani-Hamed, H-C. Cheng, and L. Hall, "Flavor Mixing Signals for Realistic Supersymmetric Unification," *Physical Review D*, 53, 413–436 (1996);

T. Kosmas, G. Leontaris and J. Vergados, *Progress in Particle and Nuclear Physics*, 33, 397 (1994) and included references.

[2] R. Bolton, *et. al.*, "Search for Rare Muon Decays with the Crystal Box Detector," *Physical Review D*, 38, 2077–2101 (1988).

[3] M. D. Cooper, *et. al.*, "Construction and Performance of MEGA's Low-Mass, High-Rate Cylindrical MWPCs," *Nuclear Instruments and Methods in Physics Research A*, 417, 24–49 (1998).

[4] M. Barakat, *et. al.*, *Nuclear Instruments and Methods in Physics Research A*, 349, 118 (1994).

[5] Y. Chen, *et. al.*, *Nuclear Instruments and Methods in Physics Research A*, 372, 195 (1996).

[6] W. W. Kinnison, *et. al.*, "Search for $\mu^+ \rightarrow e^+\gamma$," *Physical Review D*, 25, 2846–2868 (1982).